INITIAL SINTERING KINETICS OF LITHIUM META TITANATE AT CONSTANT RATES OF HEATING

A. R. Abbasian [1,2] , M. R. Rahimipour[*,2] and Z. Hamnabard[3]

* *m-rahimi@merc.ac.ir*

Received: March 2013 **Accepted: July 2013**

[1] Material Research School, Nuclear Science and Technology Research Institute, Isfahan, Iran.

[2] Ceramic Department, Materials and Energy Research Center, Karaj, Iran.

[3] Laser and Optics Research School, Nuclear Science and Technology Research Institute, Tehran, Iran.

Abstract:*In order to evaluate the sintering behavior of lithium meta titanate (Li_2TiO_3) powder, the shrinkage of powder compact was measured under constant rates of heating. Densification curves for Li_2TiO_3 have been constructed with the help of shrinkage powder measured at different heating rates. The activation energy at the initial stage of sintering was determined by analyzing the densification curves and the value of Q=377 kJ/mol was obtained. The diffusion mechanism at the initial sintering stage was determined by the analytical method applied to the constant rates of heating data. This analysis exhibited that the dominant mechanism for initial sintering stage of Li_2TiO_3 is volume diffusion from grain boundary and surfaces.*

Keywords: *sintering, lithium meta titanate*

1. INTRODUCTION

Nuclear fusion, the process that powers the Sun, can play a big part in our carbon-free energy future. With the intention of generation of electricity the fusion base reactors are being designed and developed. Tritium is the principal fuel for future fusion power reactors. The breeding blanket is a key component of the fusion reactor because it directly involves tritium breeding and energy extraction, both of which are critical to the development of fusion power [1]. In recent years, there is a general agreement that lithium containing ceramics are the best option for tritium production and release through the 6Li+1n→(He+2.1MeV)+(T+2.7MeV) nuclear transmutation [2]. Hence, worldwide efforts have been devoted to research & development of lithium ceramic breeding blanket.

The significant candidate ceramics for this breeding blanket are lithium-containing ternary oxides, such as $LiAlO_2$, Li_2ZrO_3, Li_4SiO_4 and Li_2TiO_3 [3]. Among them, lithium meta titanate (Li_2TiO_3) has interested multitude researchers' attention for its distinguished properties as one of the most promising solid breeder materials, such as reasonable lithium atom density, low activation, high chemical stability, good compatibility with structural materials, acceptable mechanical strength and considerably good tritium release characteristics at low temperatures [4-8].

Sintered block, such as a bar or a ring, and pebble are material-form options for offline and online tritium breeders, respectively [9]. Therefore, different fabrication techniques must be established to prepare ceramic tritium breeders with different shapes. However, sintering is always the final step for the fabrication of the required parts with controlled densification and microstructural evolution. Consequently, the knowledge on the sintering mechanism and relevant parameters, such as activation energy of sintering, becomes useful [10]. With a review of the published literature we found no report dealing with mechanism of sintering for a Li_2TiO_3 material have been published so far. Therefore, we intend to explore the initial stage of sintering on Li_2TiO_3 ceramic.

The primary derivations of the initial stage sintering equations can be found in publications by Kingery and Berg [11], Coble [12], and Johnson and Cutler [13]. Following the work of previous researchers, Young and Cutler [14] have derived the sintering-rate equations that are applicable to quantitative analysis for shrinkage data measured under constant rates of heating (CRH) and estimated the activation energy to

induce diffusion at the initial sintering stage. Wang and Raj [15, 16] have derived the sintering-rate equation used for estimation of the activation energy at intermediate sintering stage by CRH technique. Matsui and co-workers [17, 18] propose a useful combination of the equation developed by Young–Cutler [14] and Wang–Raj [15, 16]. This analytical method can be used to determine the sintering mechanism at the initial sintering stage by employing a CRH technique. This procedure has been successfully applied to several studies including effect of SiO_2 [19], Al_2O_3 [17, 18, 20] and GeO_2 [21] on the initial sintering stage of fine zirconia powder. Moreover, Banerjee et al. [22] have studied the sintering kinetics of ThO_2–4%UO_2 pellet by similar procedure.

Matsui et al. [17, 18] derived two sintering equations for constant heating rate as follows.

$$Ln\left[TC\frac{d\rho}{dT}\right]=\frac{-Q}{RT}+Ln\left[f(\rho)\right]+Ln\left[\frac{K\gamma\Omega D_0}{k_b}\right]-pLn(a) \quad (1)$$

$$\frac{d\left(\Delta L/L_0\right)}{dT}=\left(\frac{K\gamma\Omega D_0 R}{ka^p CQ}\right)^n \exp\left(\frac{nQ}{RT^{2-n}}\right).\exp\left(\frac{-nQ}{RT}\right) \quad (2)$$

where T is absolute temperature, C the heating rate, $d\rho/dT$ the densification rate, Q the activation energy, R the universal constant of gases, $f(\rho)$ the function of density, K the numerical constant, γ the surface energy, Ω the atomic volume, D_0 the frequency factor, k_b the Boltzmann's constant, a the particle radius, $\Delta L(=L_0-L)$ the change in length of the compacts, L_0 the initial length of the compacts, and the parameters n and p the order depending on the diffusion mechanism. Eqs. (1) and (2) is applicable to the fractional shrinkages of <4%, which fulfill the initial or early stage sintering condition. Reader could study the detailed formula deviation process by reference [18].

Using CRH experiments, the analysis method that is able to determine the diffusion mechanism at the initial sintering step is derived as follows: in Eq. (1), using the slope S_1 of the Arrhenius-type plot of $Ln\left[TC\frac{d\rho}{dT}\right]$ against $\frac{1}{T}$ at same density, the activation energy is expressed as:

$$Q = -RS_1 \quad (3)$$

In Eq. (2), using the slope S_2 of the Arrhenius-type plot of $T^{2-n}\frac{d\left(\Delta L/L_0\right)}{dT}$ against $\frac{1}{T}$, the apparent activation energy is expressed as:

$$nQ = -RS_2 \quad (4)$$

Since the n range was $n=0.31$-0.53 [23], the S_2 may be estimated from the plot of $T^{1.58}\frac{d\left(\Delta L/L_0\right)}{dT}$ against $\frac{1}{T}$. Combining Eqs. (3) and (4) we have:

$$n=\frac{nQ}{Q}=\frac{S_2}{S_1} \quad (5)$$

Eqs. (3)–(5) were used to determine the values of activation energy and diffusion mechanisms at the initial sintering step using the results of the CRH techniques.

2. EXPERIMENTAL PROCEDURE

2. 1. Raw Material

A Li_2TiO_3 powder (−325 mesh, 400939, Sigma-Aldrich, Germany) was used in this investigation. Images of scanning electron microscopy (SEM) (Philips XL-30, Netherland) of the powder at two different magnifications are shown in Fig. 1. Fig. 1 (a) exhibits the particle shape is polygonal and Fig. 1 (b) indicates severe agglomeration with different sizes occurred between the particles. Fig. 2 shows the hard agglomerate size distribution of the powder was

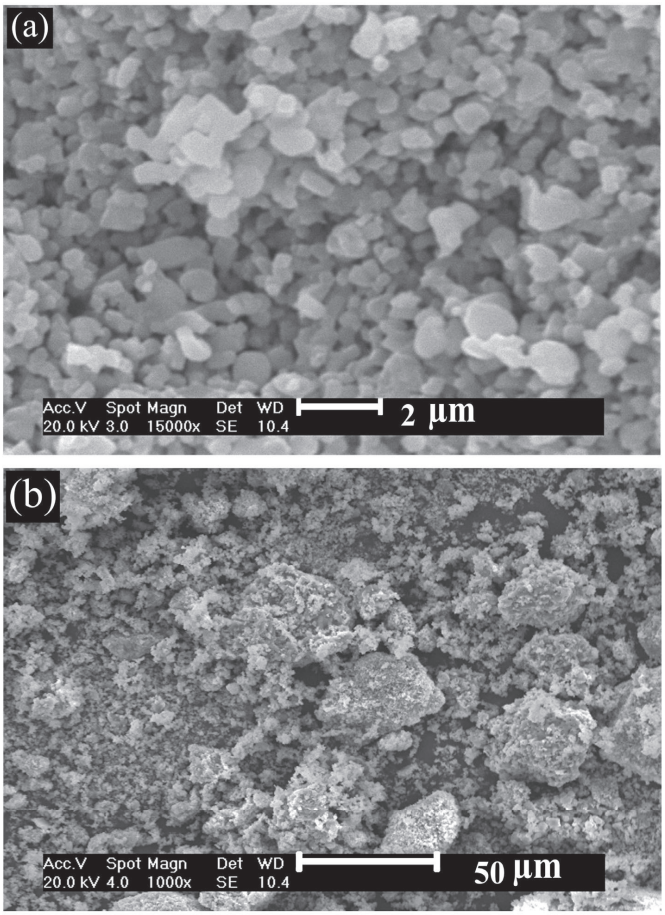

Fig. 1. (a and b) SEM analysis of Li_2TiO_3 powder at two different magnifications.

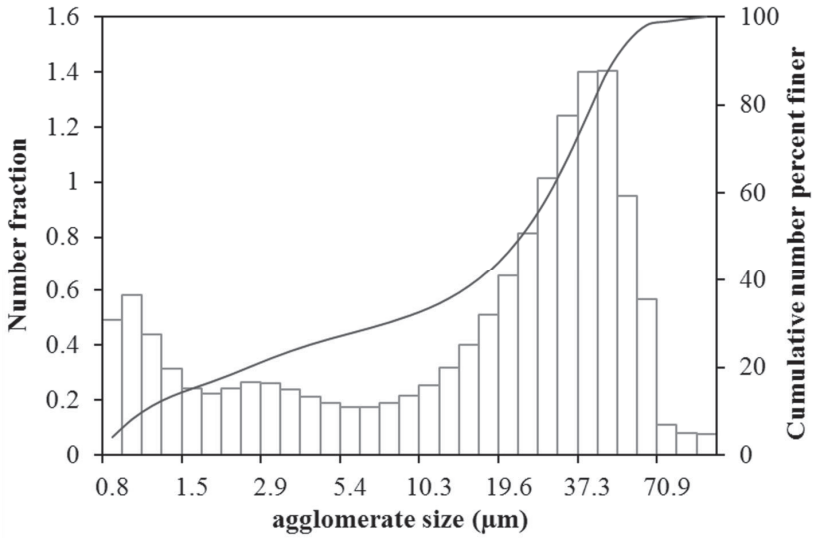

Fig. 2. The hard agglomerate size distribution of the Li_2TiO_3 powder.

determined with a laser particle size analyzer (Fritch, Analysette 22, Germany). The mean hard agglomerate size of the powder was determined at approximately 23 μm.

2. 2. Sample Preparation

The as-received powder was pressed on a hydraulic press under pressure of about 300±3 MPa at room temperature using stainless steel die to create bars of ~5×5×50 mm^3. Before proceeding to sintering, to ensure the absence of any moisture, the compact powder was dried. The green density was measured by the geometric method. The green density of Li_2TiO_3 powder compacts was 2.15±0.03 g/cm^3. The value of 3.43 g/cm^3 was used as the theoretical density.

2. 3. Dilatometry

An optical non-contact dilatometer (Misura ODLT, Expert System, ITALY) was used to study the in situ shrinkage of the powder compact during sintering in air at different heating rates. Two beams of light illuminate both the ends of a specimen 50 mm long placed horizontally into the furnace and two digital cameras capture the images of the last few hundreds microns of each tip. The specimen, completely free to expand or contract, is measured by the image that it projects on a Charge-Coupled Device (CCD). This instrument consists of a kiln equipped with an automatic temperature controller, which can reach a heating rate of 30 K per minute. The temperature increases from room temperature (RT) to 1200°C at the preset heating rate with no holding time. As a final result, the dimensional changes (expansion or shrinkage with respect to the initial size) of a material are plotted in percentage on a graph as a function of the temperature. Assuming isotropy in densification of all the specimens, the relative density of the sintered specimen (ρ_s) was calculated using the following equation [24]:

$$\rho_s = \left[\frac{1}{1 - dL/L_0 + \alpha(T - T_0)}\right]^3 \rho_g \qquad (6)$$

where dL/L_0 is instantaneous linear shrinkage obtained by the dilatometer test, L_0 is the initial length of the specimen, T is the measured temperature, T_0 is the room temperature ρ_g is the green density, and α is the coefficient of thermal expansion.

From a practical point of view, α is determined from the cooling steps of the dilatometer run. [25]. An average value α as a function of temperature, T, by the following estimation equations was determined from the cooling steps of the dilatometer runs performed with the different heating rate adopted during our investigations.

$$\alpha(K^{-1}) = 1.4635\times10^{-5} + 9.5499\times10^{-9}T - 4.3946\times10^{-12}T^2 \quad (25<T<1360\,K) \qquad (7)$$

$$\alpha(K^{-1}) = 1.9820\times10^{-5} \quad (T \geq 1360\,K) \qquad (8)$$

The final densities after the dilatometer experiments as calculated in this way were in admissible agreement with those measured by the Archimedes technique.

3. RESULTS AND DISCUSSION

Figs. 3 and 4 show the change of the shrinkage and shrinkage rate of Li_2TiO_3 compact during non-isothermal sintering at five different heating rates of 2, 3.5, 10, 20 and 30 K min^{-1}, respectively. For each heating rate, the compacts show the normal linear expansion behaviors and then a tendency to shrink. The comparative data of the sintering response is summarized in Table 1.

Table 1. Dilatometry data for Li_2TiO_3 powder compact sintered at different heating rates.

Heating rate (K min^{-1})	T_{Onset} (°C)	T_{max} (°C)
2	825	1014
3.5	846	1025
10	882	1052
20	890	1078
30	909	1094

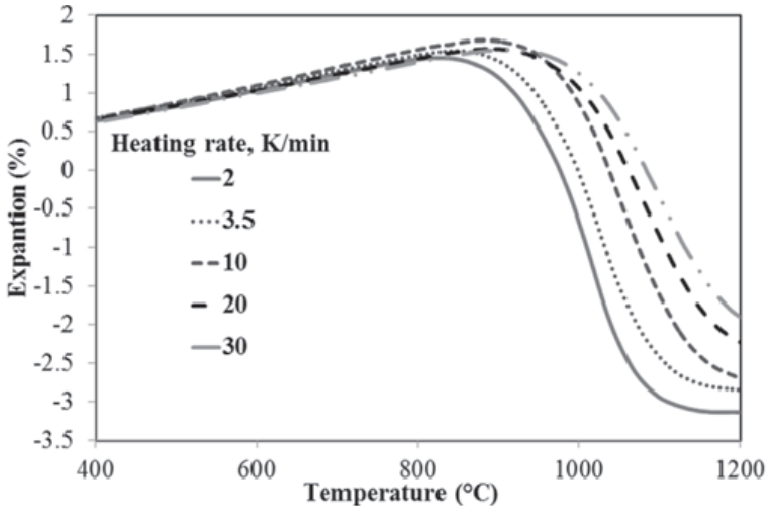

Fig. 3. Effect of heating rate on the shrinkage of Li_2TiO_3 compact as a function of temperature.

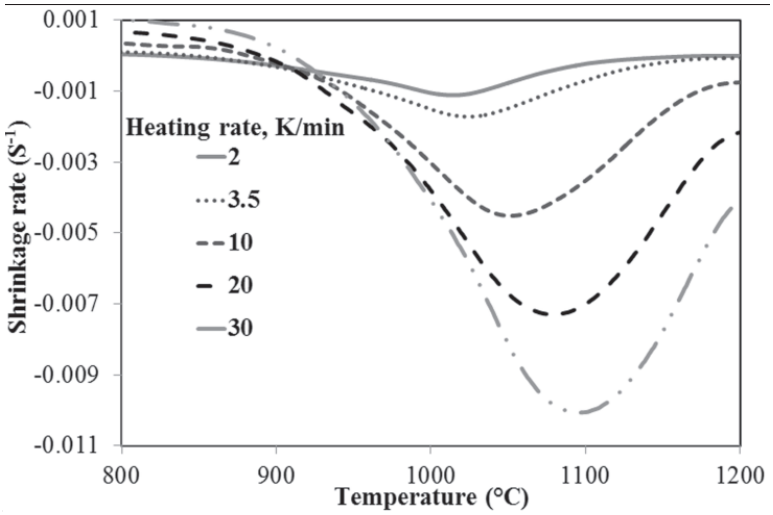

Fig. 4. Effect of heating rate on the shrinkage rate of Li_2TiO_3 compact as a function of temperature.

Apparently, increasing the heating rate increased the temperatures at which sintering starts (arbitrary set to 0.5% shrinkage, T_{Onset}) and proceeds. For instance, T_{Onset} occurred at 825 and 909 °C when heating rates increased from 2 to 30 K min^{-1}. This kind of behavior is not new and has been previously observed for ThO_2–4%UO_2 [22] and ThO_2 [26] nuclear ceramic powders. However, this does not absolutely mean that the densification mechanism is modified. It is more related to a kinetic aspect. For interpreting this tendency, it is invoked that, at a lower heating rate, a compact is exposed for a longer time and shrinks more until reaching a certain temperature (for instance T_{Onset}) [27]. For the same reason, the shrinkage rate curves of specimens shifted to higher temperature, as the heating rate increased. The maximum shrinkage rate was found to be dependent on heating rate, i.e. the higher the heating rate, the higher is the instantaneous

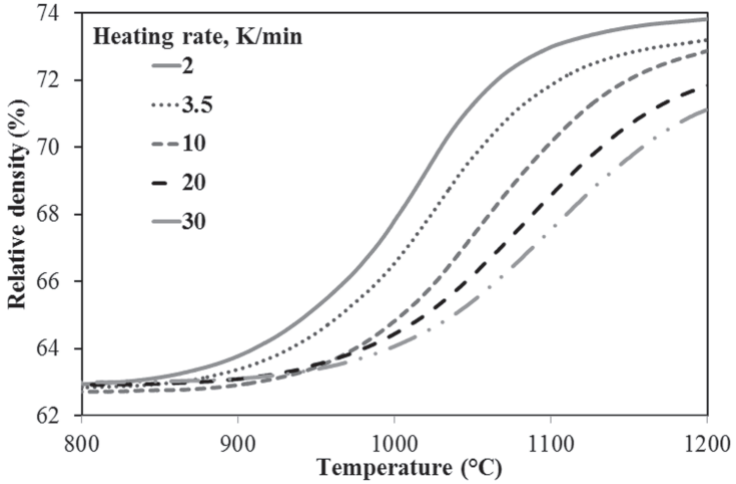

Fig. 5. Relative density of Li_2TiO_3 compacts as a function of temperature during nonisothermal sintering at different heating rates.

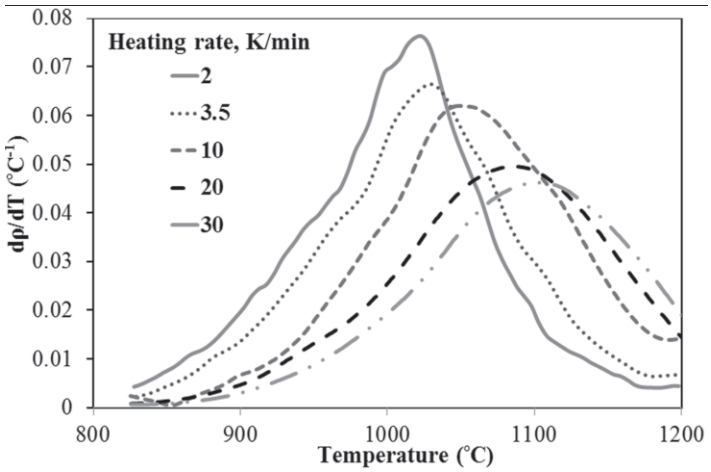

Fig. 6. Temperature dependence of densification rate of Li_2TiO_3 in the course of heating 2-30 $Kmin^{-1}$.

shrinkage rate whatever is the temperature. This tendency is also well known and has been previously reported in the case of Al_2O_3 [28] and 3Y-TZP [29] materials.

Shrinkage curves of Fig. 3 were replotted as percentage of theoretical density versus temperature with the help of Eq. (6). Fig. 5 shows the relative density for Li_2TiO_3 samples as a function of temperature. The density–temperature curves displayed the familiar sigmoidal shape and generally shifted to higher temperatures with increasing heating rate. It can be noted that the achieved sintered densities at any temperature showed a modest but systematic dependence on the heating rate. The maximum density was found to depend upon the heating rate, the higher the heating rate the lower the sintered density. This behavior has also have reported for zirconia [25], alumina [28], cerium oxide [30], and magnesium aluminate spinel [31] systems. It is well documented that, at a lower heating rate, the compact is exposed to sintering for a longer time

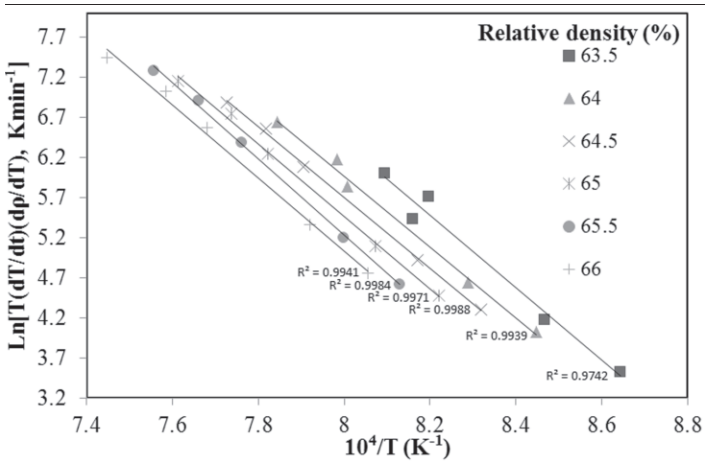

Fig. 7. Arrhenius type plots for the estimate of activation energies of sintering.

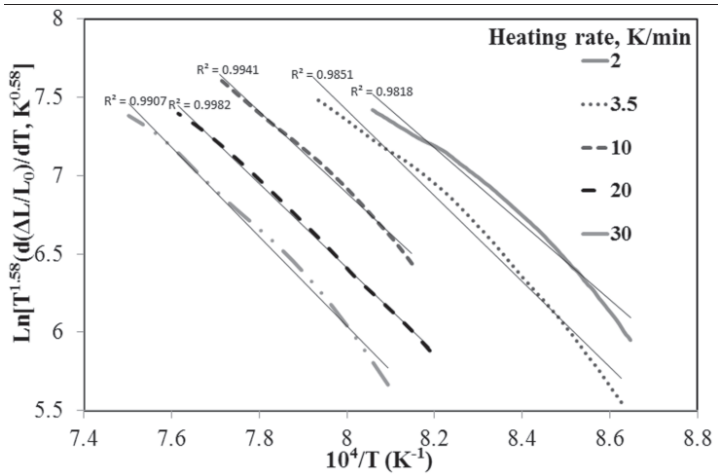

Fig. 8. Plot of $\ln[T^{1.58}\, d(\Delta L/L_0)/dT]$ against 1/T of Li_2TiO_3 at different heating rates.

during heating period; hence, the amount of shrinkage is higher.

Fig. 6 shows the temperature dependence of the densification rates ($d\rho/dT$) of Li_2TiO_3 measured at 2–30 K min^{-1} heating rates. It can be seen from Fig. 6 that with increase in heating rate, the height of the peaks increased and curves shifted to a higher temperature. Wang and Raj [15] demonstrated that a higher peak temperature and a greater height of the peak imply a larger activation energy. Therefore, position and height of the peak in $d\rho/dT$ give an immediate indication of the activation energy.

To inspect the mass-transport paths at the initial sintering stage in Li_2TiO_3, the activation energy (Q) and the apparent activation energy (nQ) of diffusion, and order on diffusion mechanism (n) can be appraised by applying Eqs. (1), (2) and (5) to the results in Figs. 3 and 4. Eq. (1) is applied in the following way. For each heating rate (dT/dt), both T and (dT/dt) at the same relative density were determined, and their values were plotted as $\ln[T(dT/dt)(d\rho/dT)]$ against 1/T (Fig. 7). Here, this analysis was executed in the relative density range of <66%, which corresponds to the fractional shrinkage range of <4%. The plot at each relative density showed a linear relation. The Q at each relative density was determined from the slope of the

Table 2. Activation energy, apparent activation energy, and order on diffusion mechanism at the initial sintering stage of the Li_2TiO_3

Activation energy		Apparent activation energy		Order on diffusion mechanism
Q (kJ/mol)	Standard deviation	*nQ* (kJ/mol)	Standard deviation	*n*
377	10	221	13	0.58

straight line and as summarized in Table 2, the average value of 377 kJ/mol was obtained. On the other hand, Eq. (2) is applied in the following way. In the fractional shrinkage range of <4%, the nQ was determined from the slope of the straight line in the plot of $\ln[T^{1.58}\, d(\Delta L/L_0)/dT]$ versus using the shrinkage curve of each heating rates. The proper plots at different heating rate are shown in Fig. 8. Linear relations were obtained at all plots of 2–30 K min^{-1} heating rates. As summarized in Table 2, the average value of 221 kJ/mol for nQ was obtained. Using the average values of both Q and nQ, the values of n were calculated by Eq. (5), which was n=0.58 (Table 2). According to two-sphere shrinkage models, the n ranges are 0.31–0.33 for grain-boundary diffusion, 0.40–0.50 for volume diffusion from grain boundary only, and 0.53 for volume diffusion from grain boundary and sphere surfaces, respectively [23]. Comparing them with the value determined here it is possible to propose a sintering mechanism. Therefore, volume diffusion from grain boundary and sphere surfaces is conceivable sintering mechanism for Li_2TiO_3.

However, the value n=0.58 is a little greater than n=0.53. This difference may be due to surface diffusion mechanism. Surface diffusion generally has a low activation energy; it is expected to contribute to material transport at temperatures at or below the initial shrinkage temperature. Young and Cutler [14] have reported that surface diffusion effects can be recognized in the CRH data by observing that, if a neck is

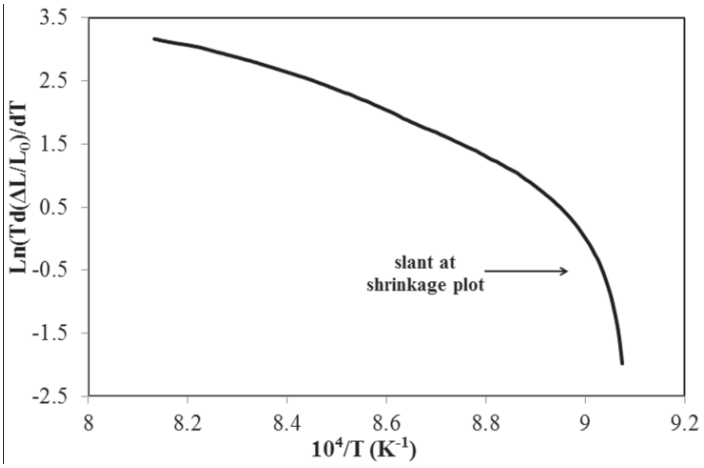

Fig. 9. Plot of $\ln[Td(\Delta L/L_0)/dT]$ against 1/T of Li_2TiO_3 in the course of heating 2 $Kmin^{-1}$.

formed by surface-diffused material, the flow of material from the grain boundary, which normally would form the neck, is impeded until a temperature is reached at which flow from the grain boundary predominates. Because of the lengthened diffusion path and larger neck radius, the rate of shrinkage is retarded until a higher temperature is reached. As diffusion from the grain boundary overpowers surface diffusion, which is not as sensitive to temperature, diffusion from the grain boundary reaches the magnitude it would have reached if no surface diffusion had occurred. The net effect is a steepened initial slope. As an example, graph of $\ln[Td(\Delta L/L_0)/dT]$ against 1/T, for initial step shrinkage of Li_2TiO_3 at 2 K min^{-1} heating is shown in Fig. 9. As can be seen from this graph, there is a slant at shrinkage plot that may be concern to surface diffusion enhancing neck growth.

4. CONCLUSIONS

Sintering in air of Li_2TiO_3 powder has been investigated by the way of dilatometer tests. Using the constant rates of heating technique and applying the analytical method to the results of measurements, it has been found that the dominant mechanism controlling densification of Li_2TiO_3 at the initial sintering stage is volume diffusion from grain boundary and surfaces with activation energy value as Q=377 kJ/mol.

ACKNOWLEDGMENTS

This work was supported by the Nuclear Science and Technology Research Institute, and the Materials and Energy Research Center (no. 389052).

REFERENCES

1. Johnson, C. E., "Ceramic breeder materials", Ceram. Int., 1991; 17: 253-258.
2. Deptula, A., Brykala, M., Lada, W., Olczak, T., Sartowska, B., Chmielewski, A.G., Wawszczak, D., Alvani, C., "Preparation of spherical particles of Li_2TiO_3 (with diameters below 100 μm) by sol-gel process", Fusion. Eng. Des., 2009; 84: 681-684.
3. Yamaguchi, K., Suzuki, A., Tonegawa, M., Takahashi, Y., Yasumoto, M., Yamawaki, M., "Hydrogen atmosphere effect on vaporization of lithium-based oxide ceramics by means of high temperature mass spectrometry and work function measurement", J. Mass Spec. Soc. Jpn., 1999; 47: 10-15.
4. Miller, J. M., Hamilton, H. B., Sullivan, J. D., "Testing of lithium titanate as an alternate blanket material", J. Nucl. Mater., 1994; 212-215: 877-880.
5. Alvani, C., Casadio, S., Contini, V., Bartolomeo, A. Di, Lulewicz, J. D., Roux, N., "Li_2TiO_3 pebbles reprocessing, recovery of 6Li as Li_2CO_3", J. Nucl. Mater., 2002; 307-311: 837-841.
6. Kopasz, J. P., Miller, J. M., Johnson, C. E., "Tritium release from lithium titanate, a low-activation tritium breeding material", J. Nucl. Mater., 1994; 212-215: 927-931.
7. Kleykamp, H., "Chemical reactivity of SiC fibre-reinforced SiC with beryllium and lithium ceramic breeder materials", J. Nucl. Mater., 2000; 283-287: 1385-1389.
8. Roux, N., Avon, J., Floreancing, A., Mougin, J., Rasneur, B., Ravel, S., "Low-temperature tritium releasing ceramics as potential materials for the ITER breeding blanket", J. Nucl. Mater., 1996; 233-237: 1431-1435.
9. Wen, Z., Wu, X., Xu, X., Lin, J., Gu, Z., "Research on the preparation of ceramic tritium breeders in SICCAS", Fusion. Eng. Des., 2010; 85: 1551-1555.
10. Song, X., Lu, J., Zhang, T., Ma, J., "Two-stage master sintering curve approach to sintering kinetics of undoped and Al_2O_3-doped 8 mol% yttria-stabilized cubic zirconia", J. Am. Ceram. Soc., 2011; 94: 1053-1059.
11. Kingery, W. D., Berg, M., "Study of the initial stages of sintering solids by viscous flow, evaporation-condensation, and self-diffusion", J. Appl. Phys., 1955; 26: 1205-1212.
12. Coble, R. L., "Initial sintering of alumina and hematite", J. Am. Ceram. Soc., 1958; 41: 55-62.
13. Johnson, D. L., Cutler, I. B., "Diffusion sintering: I, initial stage sintering models and their application to shrinkage of powder compacts", J. Am. Ceram. Soc., 1963; 46: 541-545.
14. Young, W. S., Cutler, I. B., "Initial sintering with constant rates of heating", J. Am. Ceram.

Soc., 1970; 53: 659-663.
15. Wang, J., Raj, R., "Estimate of the activation energies for boundary diffusion from rate-controlled sintering of pure alumina, and alumina doped with zirconia or titania", J. Am. Ceram. Soc., 1990; 73: 1172-1175.
16. Wang, J., Raj, R., "Activation energy for the sintering of two-phase alumina/zirconia ceramics", J. Am. Ceram. Soc., 1991; 74: 1959-1963.
17. Matsui, K., Ohmichi, N., Ohgai, M., Enomoto, N., Hojo J., "Sintering kinetics at constant rates of heating: Effect of Al_2O_3 on the initial sintering stage of fine zirconia powder", J. Am. Ceram. Soc., 2005; 88: 3346-3352.
18. Matsui, K., Tanaka, K., Enomoto, N., Hojo J., "Sintering kinetics at constant rates of heating: Effect of alumina on the initial sintering stage of yttria-stabilized cubic zirconia powder", J. Ceram. Soc. Jpn., 2006; 114: 763-768.
19. Matsui, K., "Sintering kinetics at constant rates of heating: Mechanism of silica-enhanced sintering of fine zirconia powder", J. Am. Ceram. Soc., 2008; 91: 2534-2539.
20. Suárez, G., Sakka, Y., "Effect of alumina addition on initial sintering of cubic ZrO_2 (8YSZ)", Ceram. Int., 2010; 36: 879-885.
21. Matsui, K., Hojo, J., "Sintering kinetics at constant rates of heating: Effect of GeO_2 addition on the initial sintering stage of 3 mol% Y_2O_3-doped zirconia powder", J. Mater. Sci., 2008; 43: 852-859.
22. Banerjee, J., Kutty, T. R. G., Kumar, A., Kamath, H. S., Banerjee, S., "Densification behaviour and sintering kinetics of ThO_2-4%UO_2 pellet", J. Nucl. Mater., 2011; 408: 224-230.
23. Johnson, D. L., "New method of obtaining volume, grain-boundary, and surface diffusion coefficients from sintering data", J. Appl. Phys., 1969; 40: 192-200.
24. Ran, S., Winnubst, L., Wiratha, W., Blank, D.H.A., "Sintering behavior of 0.8 mol%-cuo-doped 3Y-TZP ceramics", J. Am. Ceram. Soc., 2006; 89: 151-155.
25. Bernard-Granger, G., Guizard, C., "Apparent activation energy for the densification of a commercially available granulated zirconia powder", J. Am. Ceram. Soc., 2007; 90: 1246-1250.
26. Kutty, T. R. G., Khan, K. B., Hegde, P. V., Banerjee, J., Sengupta, A. K., Majumdar, S., Kamath, H. S., "Development of a master sintering curve for ThO_2", J. Nucl. Mater., 2004; 327: 211-219.
27. Sato, E., Carry, C., "Yttria doping and sintering of submicrometer-grained α-alumina", J. Am. Ceram. Soc., 1996; 79: 2156-2160.
28. Aminzare, M., Golestani-fard, F., Guillon, O., Mazaheri, M., Rezaie, H. R., "Sintering behavior of an ultrafine alumina powder shaped by pressure filtration and dry pressing", Mater. Sci. Eng. A, 2010; 527: 3807-3812.
29. Mazaheri, M., Simchi, A., Dourandish, M., Golestani-Fard, F., "Master sintering curves of a nanoscale 3Y-TZP powder compacts", Ceram. Int., 2009; 35: 547-554.
30. Kinemuchi, Y., Watari, K., "Dilatometer analysis of sintering behavior of nano-CeO_2 particles", J. Eur. Ceram. Soc., 2008; 28: 2019-2024.
31. Rozenburg, K., Reimanis, I. E., Kleebe, H. J., Cook, R. L., "Sintering kinetics of a $MgAl_2O_4$ spinel doped with LiF", J. Am. Ceram. Soc., 2008; 91: 444-450.